The Journal of Immunology

Targeted Delivery of Curcumin Rescues Endoplasmic Reticulum–Retained Mutant NOX2 Protein and Avoids Leukocyte Apoptosis

Chia-Liang Yen, Yi-Chu Liao, Ru-Fen Chen, Ya-Fang Huang, Wan-Chen Chung, Pei-Chi Lo, Chuan-Fa Chang, Ping-Ching Wu, Dar-Bin Shieh, Si-Tse Jiang and Chi-Chang Shieh

J Immunol 2019; 202:3394-3403; Prepublished online 13 May 2019;
doi: 10.4049/jimmunol.1801599
http://www.jimmunol.org/content/202/12/3394

The Journal of Immunology is published twice each month by
The American Association of Immunologists, Inc.,
1451 Rockville Pike, Suite 650, Rockville, MD 20852

Print ISSN: 0022-1767 Online ISSN: 1550-6606.

Targeted Delivery of Curcumin Rescues Endoplasmic Reticulum–Retained Mutant NOX2 Protein and Avoids Leukocyte Apoptosis

Chia-Liang Yen,* Yi-Chu Liao,* Ru-Fen Chen,† Ya-Fang Huang,‡ Wan-Chen Chung,* Pei-Chi Lo,§ Chuan-Fa Chang,¶ Ping-Ching Wu,‖ Dar-Bin Shieh,†,#, Si-Tse Jiang,‡ and Chi-Chang Shieh*,††**

Chronic granulomatous disease (CGD) is a primary immunodeficiency disease caused by defects in the leukocyte NADP oxidase. We previously reported that sarcoplasmic/endoplasmic reticulum calcium pump (SERCA) inhibitors could be used to rescue mutant H338Y-gp91phox protein of a particular type of CGD with a *Cybb*^{C1024T} mutation, leading to endoplasmic reticulum (ER) retention of the mutant protein. In this study, we developed a novel mouse model with the *Cybb*^{C1024T} mutation on a Cybb knockout background and investigated the therapeutic effects of ER-targeted delivery of the SERCA inhibitor, curcumin, with poly(lactic-coglycolic acid) (PLGA) nanoparticles (NPs). We found that PLGA encapsulation improved the efficacy of curcumin as a SERCA inhibitor to induce ER calcium release. ER-targeting curcumin-loaded PLGA NPs reduced and delayed extracellular calcium entry and protected the cells from mitochondrial damage and apoptosis. In vivo studies showed that ER-targeting curcumin-loaded PLGA NPs treatment enhanced neutrophil gp91phox expression, ROS production and peritoneal bacterial clearance ability of the *Cybb*^{C1024T} transgenic *Cybb*$^{-/-}$ mice. Our findings indicate that ER-targeted delivery of curcumin not only rescues ER-retained H338Y-gp91phox protein, and hence leukocyte function, but also enhances the bioavailability and reduces cytotoxicity. Modulation of ER function by using organelle-targeted NPs may be a promising strategy to improve the therapeutic potential of curcumin as a treatment for CGD. *The Journal of Immunology*, 2019, 202: 3394–3403.

Chronic granulomatous disease (CGD) is a primary immunodeficiency disease (PIDD) caused by defects in the NADP (NADPH) oxidase in the leukocytes (1–3). Phagocytic NADPH oxidase (NOX2), which mediates the massive production of reactive oxygen species (ROS) by stimulated leukocytes, is composed of membrane-bound and cytosolic subunits (2). The membrane-bound subunits of NOX2 comprise gp91^{phox} and p22^{phox}, whereas the cytosolic components include p40^{phox}, p47^{phox}, p67^{phox}, and small GTPase Rac1/2. CGD patients, who have mutations in the genes encoding NOX2, are susceptible to various infections and certain autoimmune diseases due to a lack of ROS production by activated leukocytes (4–6). Currently, hematopoietic stem cell transplantation (HSCT) is the only curative treatment for CGD, whereas successful gene therapies have been reported in some cases (7–10). Given the high costs and risks of HSCT and gene therapy, treatment aimed at restoring defective leukocyte function would have a large impact on CGD patients. However, therapies to directly ameliorate the compromised ROS-producing function of NOX2 in CGD patients is still lacking.

In our previous studies, we identified a CGD patient with a point mutation (C1024T) in the *Cybb* gene, which encodes gp91^{phox} protein (11). The mutant protein contains a single amino acid change (H338Y) at the flavin adenine dinucleotide (FAD)-binding site and exists in immature forms that are retained in the endoplasmic reticulum (ER) through binding to calcium-dependent ER chaperones including calnexin. Similar to many other genetic

*Institute of Clinical Medicine, National Cheng Kung University, Tainan 70457, Taiwan; †Institute of Oral Medicine, National Cheng Kung University, Tainan 70457, Taiwan; ‡National Laboratory Animal Center, National Applied Research Laboratories, Tainan 74147, Taiwan; §Department of Surgery, Osaka University Graduate School of Medicine, Osaka 565-0871, Japan; ¶Department of Medical Laboratory Science and Biotechnology, National Cheng Kung University, Tainan 70457, Taiwan; ‖Department of Biomedical Engineering, National Cheng Kung University, Tainan 70457, Taiwan; #Department of Stomatology, National Cheng Kung University Hospital, College of Medicine, National Cheng Kung University, Tainan 70457, Taiwan; **Center for Micro/Nano Science and Technology, Advanced Optronic Technology Center, Innovation Center for Advanced Medical Device Technology, National Cheng Kung University, Tainan 70457, Taiwan; and ††Department of Pediatrics, National Cheng Kung University Hospital, College of Medicine, National Cheng Kung University, Tainan 70457, Taiwan

ORCIDs: 0000-0002-7676-5400 (C.-L.Y.); 0000-0002-9458-1445 (Y.-C.L.); 0000-0003-2404-1248 (C.-F.C.).

Received for publication December 6, 2018. Accepted for publication April 5, 2019.

This work was supported by the National Research Program Biopharmaceuticals of the Ministry of Science and Technology (105-2325-B-006 -008) (to C.-C.S. and D.-B.S.) and the Center of Applied Nanomedicine, National Cheng Kung University from the Featured Areas Research Center Program within the framework of the Higher Education Sprout Project by the Ministry of Education of Taiwan (to D.-B. S.).

C.-C.S. initiated the idea; C.-L.Y., Y.-F.H., and C.-C.S. designed the experiments; C.-L.Y., Y.-C.L., W.-C.C., and P.-C.L performed the experiments and analyzed the data; R.-F.C., C.-F.C., P.-C.W., D.-B.S., and S.-T.J. provided critical materials and reagents for the study; C.-L.Y. and C.-C.S. wrote the manuscript.

Address correspondence and reprint requests to Prof. Chi-Chang Shieh, Institute of Clinical Medicine, National Cheng Kung University Medical College, 138 Sheng-Li Road, Tainan 704, Taiwan. E-mail address: cshieh@mail.ncku.edu.tw

The online version of this article contains supplemental material.

Abbreviations used in this article: AUC, area under the curve; BAC, bacterial artificial chromosome; CGD, chronic granulomatous disease; cryo-TEM, cryogenic transmission electron microscopy; DLS, dynamic laser scattering; ER, endoplasmic reticulum; FTIR, Fourier-transform infrared spectroscopy; H2DCF-DA, 2′, 7′-dichlorofluorescein diacetate; HSCT, hematopoietic stem cell transplantation; NCKU, National Cheng Kung University; NOX2, NADPH oxidase; NP, nanoparticle; NR, Nile Red; PIDD, primary immunodeficiency disease; PLGA, poly(lactic-coglycolic acid); SERCA, sarcoplasmic/ER calcium pump; STIM1, stromal interaction molecule 1; TMRM, tetramethylrhodamine; UPR, unfolded protein response; WT, wild-type.

diseases, this ER retention leads to protein degradation by the unfolded protein response (UPR) and is responsible for the poor cellular function (11). By modulating ER calcium levels through inhibiting ER membrane sarcoplasmic/ER calcium pump (SERCA), which maintains the high calcium concentration in the ER, we may facilitate the dissociation the mutant protein from the chaperon, release it from the ER, and restore protein function (12). To address ER retention of H338Y- gp91^{phox} and rescue leukocyte function, we previously treated CGD leukocytes with a SERCA inhibitor, thapsigargin. We found that thapsigargin- and FAD-treated *Cybb*^{C1024T} CGD leukocytes expressed more mature gp91^{phox} and had enhanced bactericidal ability (13).

Curcumin is a low m.w. dietary polyphenolic compound with SERCA inhibitory properties (14–16). Previous studies have shown that curcumin partially corrects ER retention of mutant proteins in cells with cystic fibrosis mutations (17). However, it has been shown that curcumin has multiple intracellular targets other than SERCA and induces cytotoxic side effects including ER stress and apoptosis (18–20). The application of curcumin as a therapeutic agent has been further limited by its poor bioavailability as curcumin has low water solubility and rapid degradation rates in vivo (21). To improve the bioavailability and efficacy of curcumin, nanoparticle (NP)-encapsulated curcumin has been investigated in in vivo and in vitro experiments (22, 23). In this study, we developed poly(lactic-coglycolic acid) (PLGA) NP-based delivery vehicles for curcumin and tested their ability to rescue mutant H338Y- gp91^{phox} protein in a novel mouse model with the disease-causing *Cybb*^{C1024T} mutation that mimics the immunodeficiency of human CGD patients. We also investigated the efficacy of curcumin as a SERCA inhibitor with curcumin encapsulated in ER-targeting peptide-decorated PLGA nanovehicles. Furthermore, the cytotoxic side effects induced by free curcumin and its nanoformulations were analyzed to investigate the therapeutic potentials of organelle-targeting delivery of NP-encapsulated curcumin.

Materials and Methods

Reagents and Abs

RPMI1640, FBS, 2′, 7′-dichlorofluorescein diacetate (H_2DCF-DA), Fluo-4 AM, ER-Tracker (Green, Blue-White DPX), tetramethylrhodamine (TMRM), and PE Annexin V Apoptotic Cell Detection kit were purchased from Invitrogen (556421; Grand Island, NY). Abs used for immunoblotting, including anti-Bip (3177), anti–phospho-ERK (4370), anti–total ERK (4695), and anti–cleaved caspase 3 (9661), were obtained from Cell Signaling (Danvers, MA). Anti-mouse gp91^{phox} (611414) and allophycocyanin-conjugated rat anti-mouse Ly6G (560599) were purchased from BD Biosciences. The eight-well slides were purchased from ibidi (Planegg, Germany).

Mice

C57BL/6 mice were used as wild-type (WT) mice and purchased from Animal Center, National Cheng Kung University (NCKU), Tainan, Taiwan. The *Cybb* knockout mice (B6.129S-*Cybb*^{tm1Din}/J, No. 002365) were purchased from The Jackson Laboratory. All mice were routinely backcrossed to the C57BL/6 background and underwent genome-wide genotyping to confirm the genetic background and were housed in the animal facility of the Laboratory Animal Center at NCKU. For peritoneal neutrophil isolation, mice were i.p. injected with 3 ml of 3% of thioglycollate. Four hours later, the mice were sacrificed, and the peritoneal cavity was washed twice with 5 ml of HBSS with 2 mM EGTA. Peritoneal neutrophils were then washed with PBS for further experiments. All procedures were approved by the Institutional Animal Care and Use Committee of NCKU.

Generating mutant Cybb^{C1024T} *transgenic mice based on the bacterial artificial chromosome*

The bacterial artificial chromosome (BAC) clone of mouse *Cybb* gene was obtained from BACPAC Resources Center. BAC modification for mutant *Cybb*^{C1024T} was performed using Counter Selection BAC Modification Kit (Gene Bridges). The modified *Cybb*^{C1024T} BACs were used for pronuclear injection in *Cybb* targeted mutant B6.129S-*Cybb*^{tm1Din}/J mice. Founders and progenies carrying BAC transgene were identified by PCR from tail DNA and direct sequencing. The full-length mutant *Cybb*^{C1024T} expression was confirmed by Western blot analysis. The transgenic mice were further backcrossed with the *Cybb* knockout mice to generate the *Cybb*^{C1024T} transgenic mice on a *Cybb* knockout background.

NP preparation

PLGA NPs were prepared with a modified approach of double emulsification (W1/O/W2 emulsion) (24). PLGA used in this study was carboxyl group terminated with inherent viscosity at 0.400–0.500 dl/g (PLA/PGA = 50:50, m.w. = 60,000, Evonik 5050 DLG 4.5A Acid, Evonik, Taiwan). Briefly, 20 mg of curcumin (C1386, Sigma-Aldrich) was dissolved in 500 μl of alcohol (W1) while 150 mg of PLGA was dispersed in 10 ml of dichloromethane solvent (O). The first emulsion was sonicated with a probe-type ultrasonic vibrator (Q700 Sonicator, Fisher Scientific) with the amplitude at 30% for 120 s with 30 s pulses and 15 s rests. The mixture (W1/O) was added to 1% PVA aqueous solution (W2) and agitated to form a second emulsion (W1/O/W2) that contains PLGA NPs. The second emulsion was sonicated for 300 s with 30 s pulses and 15 s rests. The solution was then directly vacuum degassed to remove the organic solvents, and the remaining free curcumin and PVA were removed by centrifugation. The derived product was washed with MQ with high-speed centrifugation (15,000 rpm, 15 min) twice, then with single low-speed centrifugation (1000 rpm, 10 min). Conjugation of the PLGA NPs was performed at a PLGA NP/targeting peptide ratio of 1:10 under excess EDC/NHS solution for 1 h, followed by removal of excess EDC and NHS with centrifugation. The ER-targeting peptide sequence was H-Ala-Ala-Lys-Lys-Ala-Ala-Cys-Cys-Cys-OH (Yao-Hong Biotechnology, Taiwan). The PLGA NPs were then dissolved in Milli-Q water and incubated with the peptide fragments for 18 h, followed by removal of excess peptides by centrifugation and redispersal of the precipitates in aqueous solution. The prepared NPs were protected from light and stored in water at 4˚C.

NP characterization

The morphology of the PLGA NPs was visualized with cryogenic transmission electron microscopy (cryo-TEM). The vitrified specimens were prepared by a blotting procedure performed using Cryoplunge 3 System (Gatan) as instructed by the manufacturer. We placed 3 μl of the aqueous samples containing the NPs onto a glow-discharged electron microscopy grid coated with a holey carbon film that had been plasma modified to increase hydrophilicity. Then we removed excess liquid with filter papers, and a thin film of the vitrified samples in liquid ethane was cooled with liquid nitrogen. The specimen was placed on a cryo-EM sample holder (model number 636; Gatan), then transferred to the microscope, and the image was captured with a charge-coupled device camera (Model 895; Gatan) then analyzed with Gatan Microscopy Suite software (Gatan). The hydrodynamic size was measured with the dynamic laser scattering (DLS; Delsa Nano C Particle Analyzer; Beckman Coulter), and the curcumin levels in curcumin-loaded PLGA NPs were determined by measuring the optical absorption of curcumin with UV-vis spectrophotometry (NanoDrop 1000; NanoDrop Technologies) at 435 nm after dissolving the PLGA with DMSO. The Fourier-transform infrared spectroscopy (FTIR) spectrum was measured with a Nicolet Magna 860 Spectrometer and Spectra Tech Continuum IR Microscope (Nicolet 6700; Thermo-Fisher Scientific, Madison, WI).

ROS production assay

Mice whole-blood granulocytes or peritoneal cells were washed with suspension buffer (1× HBSS and 5% FBS) three times and then incubated with 10 μM H2DCF-DA at 37˚C for 20 min. Cells were then incubated with 100 ng/ml PMA (Sigma-Aldrich) at 37˚C for 15 min, followed by fluorescence analysis with FACSCalibur (BD Biosciences). The results were analyzed by Flowing Software 2 and expressed as stimulation index obtained by the ratio between ROS levels in PMA-treated and untreated cells.

SDS-PAGE and Western blots

Cell lysates were harvested with 100 μl of lysis buffer (1% Triton-X100, 150 mM NaCl, 10 mM Tris base, 1 mM EDTA, 1 mM EGTA, 50× protease inhibitor mixture, pH 7.4). After 10% SDS-PAGE analysis, Western blots using different Abs (anti-gp91phox, Bip, phospho-ERK, total ERK, and β-actin) were performed. The signal was developed with ECL reagents. For quantitative analysis, images were analyzed with ImageJ.

Cell culture and treatment

The HL-60 cells were cultured at 37˚C in RPMI 1640 supplemented with 10% heat-inactivated FBS. DMSO (Sigma-Aldrich) at 1.3% was used to differentiate HL-60 in the density of 3 × 10^5 cells/ml. After 4 d of

incubation, differentiated cells were harvested, and dead cells were removed by Ficoll-Paque centrifuge. Differentiated HL-60 were treated with 0.5 and 10 μM of curcumin, curcumin-loaded PLGA NP, or ER-targeting curcumin-loaded PLGA NP at 1×10^6 cells/ml for 24 h.

Intracellular calcium levels and confocal microscopy

Differentiated HL-60 cells were pretreated with different concentrations of curcumin, curcumin-loaded PLGA NP, and ER-targeting peptide-decorated curcumin-loaded PLGA NP at 37°C. After overnight incubation, cells were washed with calcium-free HBSS and seeded on poly-lysine–coated eight-well slide (ibidi) on the density of 1 million cells per millimeter at 37°C for 30 min. Next, cells were labeled with 2 μM of Fluo-4 AM and 1 μM of ER-Tracker Blue-White DPX at 37°C for 30 min. The fluorescence images were captured every 10 s for 5 min with 1.25 mM of $CaCl_2$ treatment by Nikon C1-Si confocal microscopy (Nikon, Tokyo, Japan). Fluorescence intensity was analyzed using ImageJ and presented as $\Delta F/F_0$ ratio after background subtraction, where ΔF was the change in fluorescence intensity and F_0 was the baseline before $CaCl_2$ treatment. The rate of calcium level increase was shown as the differentiation of the curve. The overall calcium flux was analyzed as the area under the curve (AUC). For the detection of intracellular curcumin-loaded PLGA NP, the fluorescence signal curcumin with excitation wavelength at 488 nm was observed.

Mitochondrial membrane potential measurement

Cells treated with 0.5 or 10 μM of curcumin, curcumin-loaded PLGA NP, or ER-targeting curcumin-loaded PLGA NP for 24 h were incubated with 250 nM of mitochondrial membrane potential indicator TMRM at 37°C for 30 min. The mitochondrial membrane potential was then determined by flow cytometry and Flowing Software 2 analysis software.

Apoptotic cell detection

Cells treated with 0.5 or 10 μM of curcumin, curcumin-loaded PLGA NP, or ER-targeting curcumin-loaded PLGA NP for 24 h were washed with ice-cold PBS. Cells were then stained with PE–Annexin V, 7-AAD, or both at room temperature for 15 min. Stained cells were then suspended with binding buffer supplied by the manufacturer. The percentage of Annexin V^+ apoptotic cells were then analyzed with flow cytometry and Flowing Software 2 analysis software.

Bacterial culture and peritoneal bacterial clearance test

Frozen culture of *Staphylococcus aureus* (No. 25923; ATCC) was subcultured on a tryptic soy agar (TSA) plate with 10% sheep blood and incubated at 37°C overnight. A single colony was picked from the plate and subcultured in the Luria-Bertani medium at 37°C for 16 h. The bacterial culture was 1:50 diluted with 5ml Luria-Bertani medium and incubated at 37°C for 6 h for refreshing the bacteria. The CFU of *S. aureus* was determined by counting CFU in a 10-μl drop of cell suspension on each quarter of TSA plate. For bacterial clearance test, WT and $Cybb^{C1024T}$ transgenic $Cybb^{-/-}$ mice were injected with 1×10^7 CFU of *S. aureus* in 100 μl of PBS at peritoneum. Injected mice were sacrificed 6 h after injection, and peritoneal fluid was harvested with 5 ml of PBS. The CFU was determined by counting CFU in a 50-μl drop of cell suspension on TSA plates.

Statistical analysis

Statistical analyses were carried out with Prism software (GraphPad Software). The mean values from each group were presented as means ± SEM and compared by using one-way ANOVA or two-way ANOVA. In all tests, p values <0.05 were considered statistically significant.

Results

Generation of $Cybb^{C1024T}$ *transgenic* $Cybb^{-/-}$ *mice*

To investigate the efficacy of this novel curcumin delivery system to rescue the function of ER-retained mutant proteins, we first established a BAC transgenic mice strain, which expresses the H338Y mutant $gp91^{phox}$ protein in *Cybb* knockout background, as a novel model of human CGD (Fig. 1A). The presence of the mutation in mice was confirmed by sequencing (Fig. 1B). To confirm the expression of the mutant $gp91^{phox}$ protein, we isolated whole blood granulocytes and detected $gp91^{phox}$ protein by SDS-PAGE and Western blotting (Fig. 1C). We found that in comparison with neutrophils of $Cybb^{-/-}$ mice, granulocytes isolated from $Cybb^{C1024T}$ transgenic $Cybb^{-/-}$ mice produced underglycosylated forms of $gp91^{phox}$. As expected, the levels of the glycosylated form of the $gp91^{phox}$ protein (60–90 kDa) were lower in $Cybb^{C1024T}$ transgenic $Cybb^{-/-}$ mice than the levels in WT mice. Defected PMA-induced ROS production was also found in granulocytes isolated from $Cybb^{C1024T}$ transgenic $Cybb^{-/-}$ mice (Fig. 1D). These results indicate that we successfully established a CGD mice model with trafficking-defective $gp91^{phox}$ protein expression that mimics human CGD patients with $Cybb^{C1024T}$ mutation (11).

ER-targeting peptide facilitates the localization of curcumin-containing NPs in the ER region

We then characterized the properties of the curcumin-loaded PLGA NPs. The morphology of PLGA NPs was visualized with cryo-TEM (Fig. 2A, upper panel). The hydrodynamic diameters of the PLGA NPs obtained by DLS measurements were 255.6 ± 97.5 nm (Fig. 2A, lower panel) whereas the curcumin loading capacities in 15 independently preparations were 65.9 ± 7.8 μg/mg. The long-term observations showed that the particle size was stable for 5 mo, and the content of curcumin in the PLGA NPs was stable for up to 6 mo in distilled water (Supplemental Fig. 1).

We performed experiments to characterize the release kinetics of the curcumin-loaded PLGA NPs in different media. The results showed that 50% of the curcumin within the NPs was released when the NPs were incubated with cytoplasm mimicking buffer or with RPMI 1640 with 10% FBS at 37°C. The release was much lower in NPs incubated in distilled water or PBS at 37°C (Supplemental Fig. 2). To evaluate cellular uptake, differentiated HL-60, cortical collecting duct M-1 and human embryonic kidney 293T (HEK293T) cells were treated with 0.5 μg/ml of Nile Red (NR)–loaded PLGA NPs for 30 min, and the images were obtained with confocal microscopy (Supplemental Fig. 3A). We found that NR-loaded PLGA NPs were internalized by HL-60, M-1, and HEK293T cells. Meanwhile, whole blood lymphocytes, in contrast with $Ly6G^+$ neutrophils, did not uptake NR-loaded PLGA NPs (Supplemental Fig. 3B).

An ER-targeting peptide containing the KDEL sequence was used to decorate the PLGA NPs. After ER-targeting peptide conjugation, the hydrodynamic diameters of the decorated PLGA NPs increased to 391.2 ± 177.7 nm. The decoration process did not significantly induce curcumin release from the curcumin-loaded PLGA NPs. The FTIR spectra confirmed the decoration of ER-targeting peptide on the PLGA NPs. The ER-targeting peptide-decorated PLGA showed peaks contributed by the functional groups of carbonyl C = O stretching (~1700 cm^{-1}) and N–H bending (~1400 cm^{-1}) (25), whereas the undecorated PLGA NPs only showed the peak of C = O stretching but not the peaks at the region of N–H bending (Fig. 2B). These results indicated successful decoration of ER-targeting peptides on the PLGA NPs.

After the successful production of the curcumin-containing PLGA NPs, we went on to investigate the effects of these nanovehicles on the delivery of curcumin at the subcellular levels. Neutrophil-like–differentiated HL-60 cells were labeled with ER-Tracker and then treated with curcumin-loaded PLGA NP and ER-targeting curcumin-loaded PLGA NP. We obtained the fluorescent time-lapse images by confocal microscopy when curcumin was excited at a wavelength of 488 nm to determine the cellular distribution of curcumin-loaded PLGA NP with or without ER-targeting peptide decoration (Fig. 2C). We found that ER-targeting peptide decoration enhanced the accumulation of curcumin-loaded PLGA NP in the ER region 20' after the addition of the nanovehicles (Fig. 2C, Supplemental Videos 1, 2). The Pearson correlation coefficients of curcumin-loaded PLGA NP and ER region in cells treated with ER-targeting

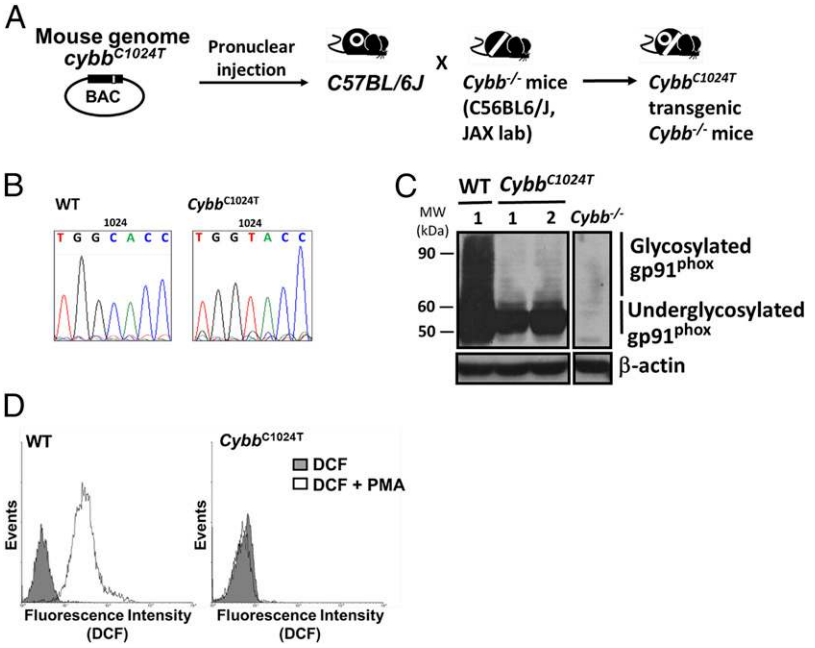

FIGURE 1. Generation of $Cybb^{C1024T}$ transgenic $Cybb^{-/-}$ mice. (**A**) The BAC containing $Cybb^{C1024T}$ mutant were microinjected into $Cybb^{-/-}$ embryo to produce $Cybb^{C1024T}$ transgenic $Cybb^{-/-}$ mice. (**B**) Sequencing results on the WT and $Cybb^{C1024T}$ transgenic $Cybb^{-/-}$ mice. (**C**) The expression of the $gp91^{phox}$ protein in neutrophils isolated from WT and two $Cybb^{C1024T}$ transgenic $Cybb^{-/-}$ mice were analyzed by SDS-PAGE and Western blots. (**D**) Neutrophils isolated from WT and $Cybb^{C1024T}$ transgenic $Cybb^{-/-}$ mice were loaded with H_2DCF-DA and treated with PMA for 10 min. PMA-induced ROS production was analyzed with flow cytometry. The experiment was performed three times with similar results.

peptide-decorated curcumin-loaded PLGA NP were significantly higher than those in cells treated with nondecorated NPs since 4' after the addition of the nanovehicles (Fig. 2D). The differences became even more significant up to 20'. These results indicate that ER-targeting peptide enhances the delivery of curcumin-loaded PLGA NP to the ER region of the cells.

NPs decorated with ER-targeting peptide enhanced the efficiency of curcumin-induced ER calcium release

We then investigated the effects of ER-targeting NP delivery on curcumin-mediated SERCA inhibition. Differentiated HL-60 cells were loaded with intracellular calcium indicator Fluo-4 AM and then treated with 0.5, 1, or 10 μM of free curcumin, curcumin-loaded

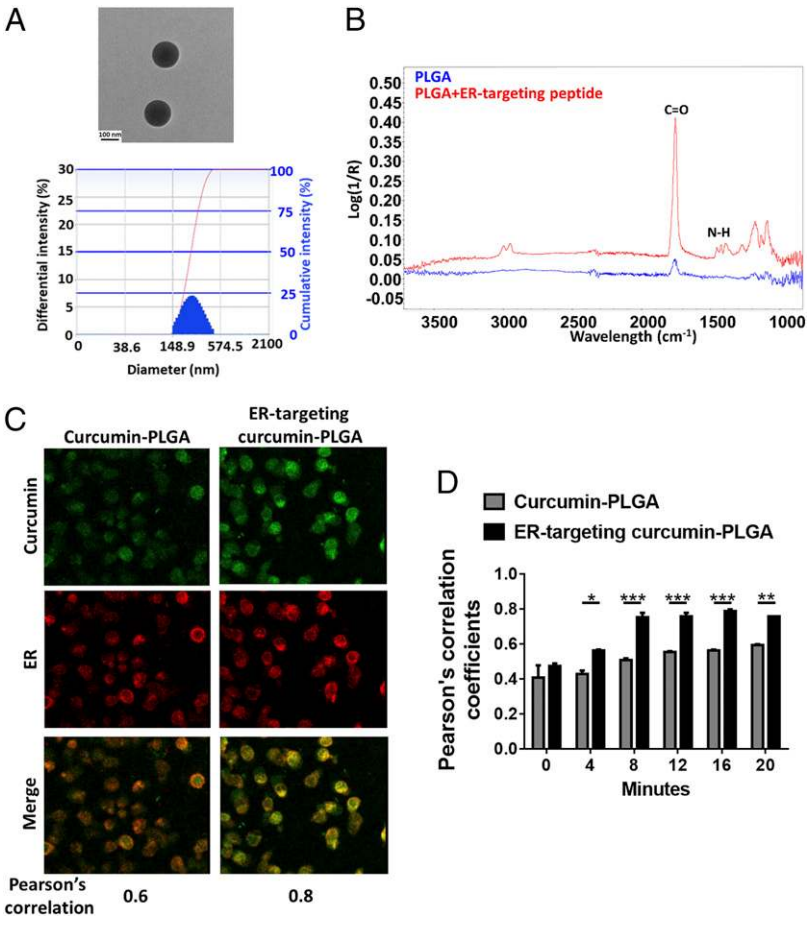

FIGURE 2. ER-targeting peptide decoration enhanced the accumulation of curcumin-containing NPs in the ER region. (**A**) Representative cryo-TEM image (upper panel) and the DLS measurement (lower panel) of the PLGA NPs. The DLS measurement was representative of 15 independent NP preparations. (**B**) FTIR spectra of PLGA NPs and ER-targeting peptide-decorated PLGA NPs after subtraction of the buffer spectrum (blue, PLGA NPs; red, ER-targeting PLGA NPs). (**C**) Differentiated HL-60 cells seeded on eight-well slide were stained with ER-Tracker and treated with curcumin-loaded PLGA NPs (10 μM) with or without ER-targeting peptide decoration. The distribution of curcumin-loaded PLGA NPs in treated cells was detected with confocal microscopy at excitation wavelength at 488 nm (original magnification ×1000). A representative result at 20 min from three independent experiments was shown. The Pearson correlation coefficients of curcumin-loaded PLGA NPs and ER region in time-lapse images of three independent experiments were analyzed and shown in (**D**) ($n = 3$; $^*p < 0.05$, $^{**}p < 0.01$, $^{***}p < 0.001$).

PLGA NP, and ER-targeting peptide-decorated curcumin-loaded PLGA NP in a calcium-free medium. The intracellular calcium levels and the ER calcium release rates were measured by detecting the changes in fluorescence intensity with confocal microscopy (Fig. 3A–C). The overall calcium release was estimated by integrating the fluorescence intensity and was shown as the AUC (Fig. 3D). We found that the fluorescence intensities in cells treated with 10 μM of curcumin at 40, 50, and 60 s were significantly higher than those of the cells treated with 0.5 or 1 μM of curcumin. (Fig. 3A, left panel). The rate of intracellular calcium increase, shown as the rate of fluorescence intensity increase, was higher in cells treated with 10 μM of curcumin in comparison with the cells treated with lower concentrations of curcumin (Fig. 3A, right panel). These findings indicate that free curcumin treatment at the concentration of 10 μM induced higher and faster ER calcium release when compared with treatments at concentrations of 0.5 and 1 μM. Meanwhile, we found no significant differences in the ER calcium release in cells treated with 0.5, 1, and 10 μM of curcumin-loaded PLGA NP or ER-targeting curcumin-loaded PLGA NP (Fig. 3B, 3C). We also compared the overall ER calcium release in cells treated with 0.5 or 10 μM of curcumin, curcumin-loaded PLGA NP, and ER-targeting curcumin-loaded PLGA NP with thapsigargin, which is a well-known SERCA inhibitor (Fig. 3D) (12, 13). We found that curcumin-loaded PLGA NP and ER-targeting curcumin-loaded PLGA NP at 0.5 μM were capable of elevating the intracellular calcium levels to the same level of thapsigargin treatment. Increasing the encapsulated curcumin to the concentration of 10 μM did not further raise the intracellular calcium level. However, free curcumin at 0.5 μM induced significantly lower ER calcium release when compared with cells treated with 0.5 μM of curcumin-loaded PLGA NP and ER-targeting curcumin-loaded PLGA NP or 10 μM of free curcumin. There were no significant changes in fluorescence intensity in untreated cells and in cells treated with empty PLGA NPs or ER-targeting PLGA NPs (data not shown). Compatible with the results in Fig. 2C and 2D showing the colocalization of NP-encapsulated curcumin in the ER, these findings suggest that NP encapsulation of curcumin at lower concentrations may induce ER calcium release to the same level as the cells treated with higher concentrations of free curcumin by more efficiently inhibiting the SERCA function in the ER.

NP-encapsulated curcumin induced weaker and delayed extracellular calcium influx

We next investigated the extracellular calcium influx, which is triggered by the depletion of ER calcium storage, in cells treated with 10 μM of free curcumin or with 0.5 μM of curcumin-loaded PLGA NP with or without ER-targeting peptide decoration for 24 h (Fig. 4A). After 24 h of treatment, cells were loaded with Fluo-4 AM under a calcium-free condition. The fluorescence images were taken before and after the addition of 1.25 mM of $CaCl_2$. A mild surge of calcium influx was observed in untreated cells when the $CaCl_2$ was added. Thapsigargin treatment at 100 nM that induced early calcium influx was used as a positive control. We found that 10 μM of free curcumin induced early extracellular calcium entry that was similar to the calcium entry induced by thapsigargin (Fig. 4A, two higher panels). In contrast, 0.5 μM of curcumin-loaded PLGA NP or curcumin-loaded PLGA NP with ER-targeting peptide decoration induced apparent extracellular calcium entry only after 60 s (Fig. 4A, two lower panels). When analyzing the calcium influx rate (Fig. 4B), we found an earlier and more robust induction of calcium entry in cells treated with thapsigargin and 10 μM of free curcumin. We found that empty NPs did not induce significant changes in the

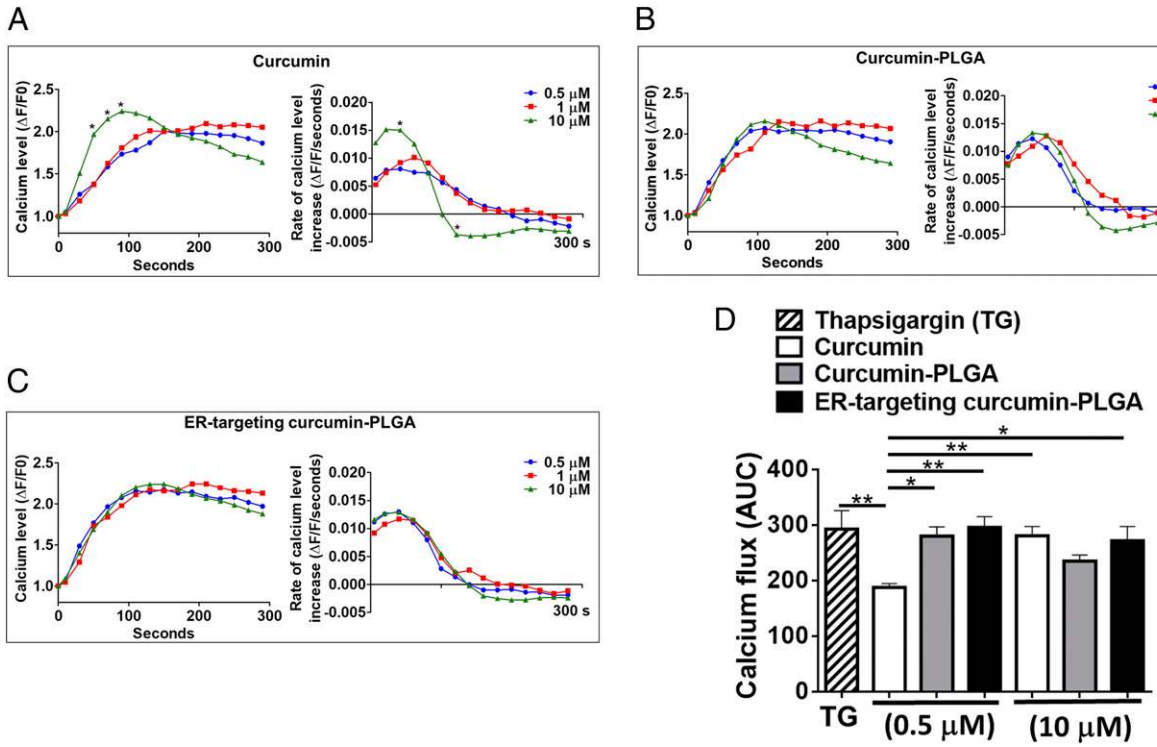

FIGURE 3. NP encapsulation and ER-targeting peptide decoration enhanced curcumin-induced ER calcium release. Differentiated HL-60 cells were seeded on eight-well slides and loaded with calcium indicator Fluo-4AM in calcium-free medium. After treatment with 0.5, 1, or 10 μM of curcumin (**A**), curcumin-loaded PLGA NP (**B**), and ER-targeting curcumin-loaded PLGA NP (**C**), the changes in fluorescence intensity within 300 s were shown in left panels. The rate of ER calcium release was estimated by differentiating the curve (right panels). The experiment was performed four times with similar results as shown in mean value ($n = 4$; $^*p < 0.05$). (**D**) The overall calcium flux was estimated as the AUC ($n = 4$; $^*p < 0.05$, $^{**}p < 0.01$).

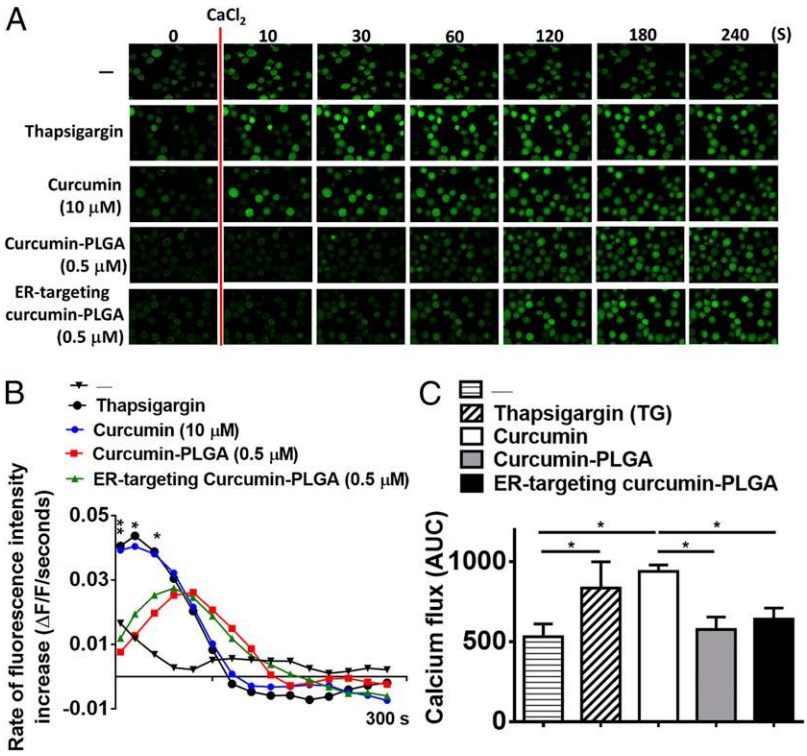

FIGURE 4. Extracellular calcium entry was delayed in cells treated with NP-encapsulated curcumin. Differentiated HL-60 cells were treated with curcumin (10 μM), curcumin-loaded PLGA NP (0.5 μM), and ER-targeting curcumin-loaded PLGA NP (0.5 μM) for 24 h. Cells were then labeled with Fluo-4 AM and seeded on eight-well slides. (**A**) The time-lapse images were captured by confocal microscopy (original magnification ×1000) before and after 1.25 μM of $CaCl_2$ treatment (red line). The images were representative of three independent experiments. (**B**) The rate of calcium flux was analyzed by differentiating the curve of the changes in fluorescence intensity. ($n = 3$; $^*p < 0.05$, $^{**}p < 0.01$). (**C**) The overall calcium flux was estimated as the AUC. ($n = 3$; $^*p < 0.05$).

fluorescence intensity when compared with untreated cells (data not shown). Despite the similar extents of ER calcium depletion induced by 10 μM of free curcumin and 0.5 μM of curcumin-loaded PLGA NP with or without ER-targeting peptide decoration (Fig. 3), the extracellular calcium entry induced by NP-encapsulated curcumin treatment was reduced regarding the influx rates and overall calcium entry in comparison with those induced by free curcumin treatment (Fig. 4B, 4C).

NP-encapsulated curcumin, especially with ER-targeting peptide decoration, induced weaker ER stress and improved cell survival in cells treated with curcumin

We next investigated whether delivery of curcumin with ER-targeting NPs affects ER stress and cell survival. There was a significant reduction in mitochondrial membrane potential in cells treated with 10 μM of free curcumin when compared with cells treated with 0.5 μM of free curcumin or curcumin-loaded PLGA NP with or without ER-targeting peptide decoration at 0.5 or 10 μM (Fig. 5A). We found a significant increase in the proportion of Annexin V^+ apoptotic cells when cells were treated with 10 μM of free curcumin (Fig. 5B). In comparison with the cells treated with 10 μM of free curcumin, the cells treated with curcumin-loaded PLGA NP and ER-targeting curcumin-loaded PLGA NP containing the same amount of curcumin showed significantly lower proportions of apoptotic cells. There were no significant differences in the percentage of Annexin V^+ cells in cells treated with curcumin-loaded PLGA NP with or without ER-targeting peptide decoration or 0.5 μM of free curcumin. There were no significant differences in mitochondrial membrane potential and the percentage of Annexin V^+ cells between untreated cells and cells treated empty NPs with or without ER-targeting peptide decoration. These findings suggest that free curcumin at a concentration that can inhibit SERCA on ER will induce rapid calcium surge to induce apoptosis, whereas NP-encapsulated curcumin with equivalent SERCA inhibition activity induces delayed calcium influx and protects the cells from mitochondrial damage and apoptosis.

To test whether the calcium imbalance and ER stress are involved in the curcumin-induced apoptosis, we examined the ER stress–related protein Bip expression and calcium-related ERK phosphorylation. We found that free curcumin and curcumin-loaded PLGA NP enhanced Bip expression and ERK phosphorylation when compared with untreated group, whereas ER-targeting peptide-decorated NPs reduced curcumin-induced Bip expression and ERK phosphorylation (Fig. 5C, 5D). Meanwhile, we found that caspase-3 cleavage, which indicates activation of apoptosis, was enhanced in cells treated with 10 μM of free curcumin. The cleavage form of caspase-3 was reduced when the curcumin was delivered with PLGA NPs with or without ER-targeting peptide decoration. Taken together, our results indicate that localizing curcumin-containing NPs to the ER region with ER-targeting peptide may reduce curcumin-induced ER stress and cell death.

Curcumin delivered with ER-targeting NPs was effective in rescuing the mutant H338Y-gp91^{phox} protein in immune cells and enhancing NOX2 function in Cybb^{C1024T} *transgenic* Cybb$^{-/-}$ *mice*

We then focused on the effects of curcumin-loaded PLGA NP with or without the ER-targeting peptide decoration on the expression and maturation of gp91^{phox} protein in *Cybb^{C1024T}* transgenic *Cybb$^{-/-}$* mice by treating the mice i.p. with different preparations with equal amounts of curcumin at 20 mg/kg. To elicit neutrophils, we collected peritoneal exudate cells from mice injected with thioglycollate for 4 h based on previous studies (26, 27). There were no significant differences in the percentages of neutrophil in thioglycollate-induced exudates from mice treated with free curcumin, curcumin-loaded PLGA NP, and ER-targeting peptide-decorated curcumin-loaded PLGA NP. We found increased expression of more maturely glycosylated forms of gp91^{phox} in thioglycollate-induced neutrophils isolated from mice treated with curcumin-loaded PLGA NP for 24 h (Fig. 6A, lane 4). ER-targeting peptide-decorated curcumin-loaded PLGA NP further improved the expression of gp91^{phox} in neutrophils isolated

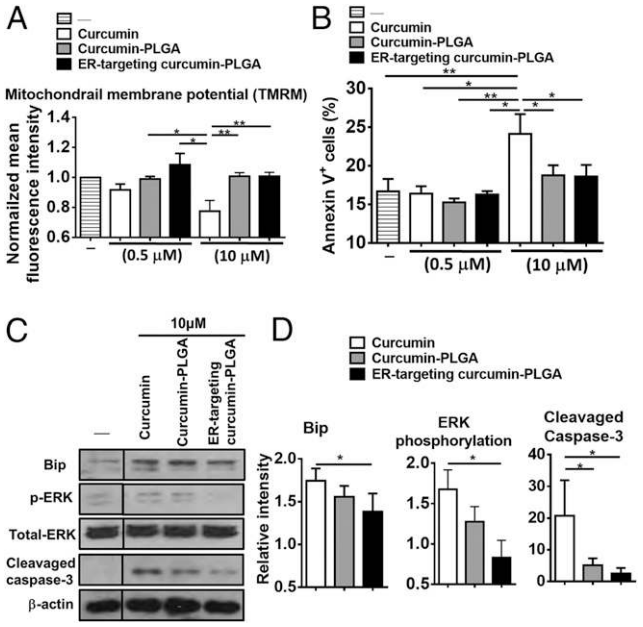

FIGURE 5. NP encapsulation downregulated curcumin-induced ER stress and apoptosis. Differentiated HL-60 cells were treated with curcumin, curcumin-loaded PLGA NP, and ER-targeting curcumin-loaded PLGA NP for 24 h. (**A** and **B**) The fluorescence intensity of TMRM and Annexin V–PE-positive cells were detected by flow cytometry ($n = 4$; $^*p < 0.05$, $^{**}p < 0.01$). (**C**) A representative image from four independent experiments showing the levels of Bip, phospho-ERK, and cleavaged-caspase-3 in lysates of treated cells. The relative intensities of the Western blot results from four independent experiments were shown in (**D**) ($n = 4$; $^*p < 0.05$).

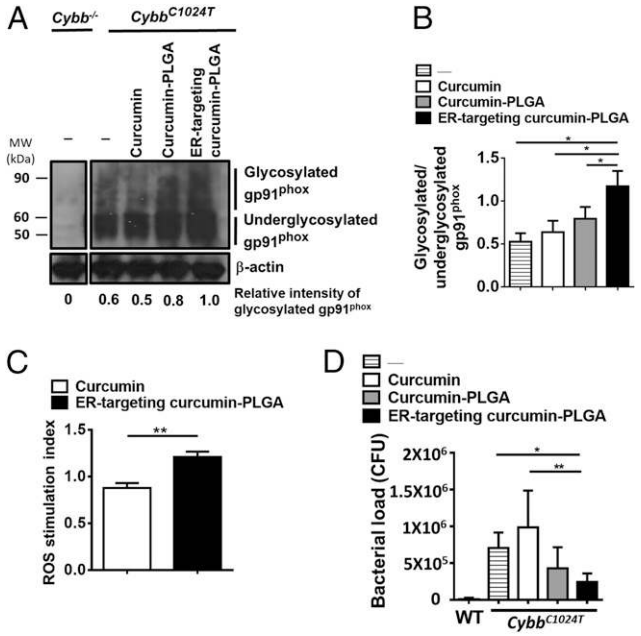

FIGURE 6. Delivery of curcumin with ER-targeting NPs rescued mutant gp91^{phox} protein glycosylation and restored neutrophil functions in *Cybb*^{C1024T} transgenic *Cybb*$^{-/-}$ mice. Neutrophils from mice treated with 20 mg/kg of free curcumin, curcumin-loaded PLGA NP, or ER-targeting curcumin-loaded PLGA NPs were isolated from thioglycollate-induced exudates. (**A**) gp91^{phox} protein expression and (**B**) relative levels of the glycosylated versus the unglycosylated form of gp91^{phox} were analyzed ($n = 4$ in each group; $^*p < 0.05$). (**C**) Neutrophils isolated from treated *Cybb*^{C1024T} transgenic *Cybb*$^{-/-}$ mice were loaded with ROS sensitive dye H_2DCF-DA. PMA-induced ROS production was analyzed with flow cytometry and was shown as ROS production index ($n = 4$ in each group; $^{**}p < 0.01$). (**D**) *Cybb*^{C1024T} transgenic *Cybb*$^{-/-}$ mice were injected i.p. with 1×10^7 CFU of *S. aureus*. After 4 h, the peritoneal cavity was lavaged to analyze the number of viable bacteria. ($n = 4$ in each group; $^*p < 0.05$, $^{**}p < 0.01$).

from treated mice (Fig. 6A, lane 5). However, there was no marked increase in the level of glycosylated gp91^{phox} in cells isolated from free curcumin-treated mice (Fig. 6A, lane 3). Similar results were found when we analyzed the ratios of glycosylated versus underglycosylated gp91^{phox} (Fig. 6B). There were no changes in gp91^{phox} glycosylation in neutrophils isolated from *Cybb*^{C1024T} transgenic *Cybb*$^{-/-}$ mice treated with empty NPs with or without ER-targeting peptide decoration. We also found higher PMA-induced ROS production in neutrophils isolated from ER-targeting peptide-decorated curcumin-loaded PLGA NP-treated mice than in cells from free curcumin-treated mice (Fig. 6C). These data suggest that treating H338Y- gp91^{phox}-expressing *Cybb*^{C1024T} transgenic *Cybb*$^{-/-}$ mice with ER-targeting nanoformulation of curcumin facilitates the maturation of mutant protein in leukocytes.

The long-term toxic effects of the curcumin-loaded PLGA NPs were also investigated. We found no significant changes in body weight (Supplemental Fig. 4A), serum urea (Supplemental Fig. 4B), serum glutamic oxaloacetic transaminase (GOT) (Supplemental Fig. 4C), and peripheral blood WBC counts (Supplemental Fig. 4D) and RBC counts (Supplemental Fig. 4E) in mice treated with empty PLGA NPs or curcumin-loaded PLGA NPs (Supplemental Fig. 4).

To test the bacterial clearance ability, we i.p. treated the *Cybb*^{C1024T} transgenic *Cybb*$^{-/-}$ mice with 20 mg/kg of free curcumin, curcumin-loaded PLGA NP, and ER-targeting peptide-decorated curcumin-loaded PLGA NP for 24 h and injected the treated mice with 1×10^7 of *S. aureus*. Four hours later, the peritoneal cavities were lavaged, and the bacterial counts (CFU) were analyzed (Fig. 6D). We found that although the WT mice had very low bacterial counts, *Cybb*^{C1024T} transgenic mice with ER-targeting peptide-decorated curcumin-loaded PLGA NP treatment had significantly lower bacteria counts when compared with the untreated or free curcumin-treated group. *Cybb*^{C1024T} transgenic *Cybb*$^{-/-}$ mice treated with empty NPs with or without ER-targeting peptide decoration showed similar bacterial counts when compared with untreated mice. Therefore, our findings indicate that ER-targeting NP-based delivery of curcumin rescues mutant gp91^{phox} protein expression and recovers NOX2 functions in mice mimicking human CGD with trafficking-defective gp91^{phox} protein expression (Fig. 7).

Discussion

Short of immune function–correcting procedures, including HSCT and gene therapy, patients with CGD are at a constant threat of severe infections due to their low production of ROS by the leukocytes (10). As some patients are not suitable for immediate function-correcting therapies because of different clinical conditions, these patients are in dire need of effective medical treatments to improve their ROS-producing functions. In this study, we showed that delivery of curcumin with ER-targeting NPs recovers NOX2 expression and function in the mice expressing the mutant *Cybb* gene encoding the ER-retained H338Y mutant gp91^{phox} protein. Our formulation of curcumin, with the combination of NPs encapsulation and surface modification, increased the efficacy of drug delivery to the target organelle (ER) and reduced the cytotoxicity at the same time. Our results strongly suggest that organelle-targeting nanovehicle may be a promising strategy to improve the therapeutic potential of curcumin as the treatment for PIDD caused by ER retention of the mutant proteins.

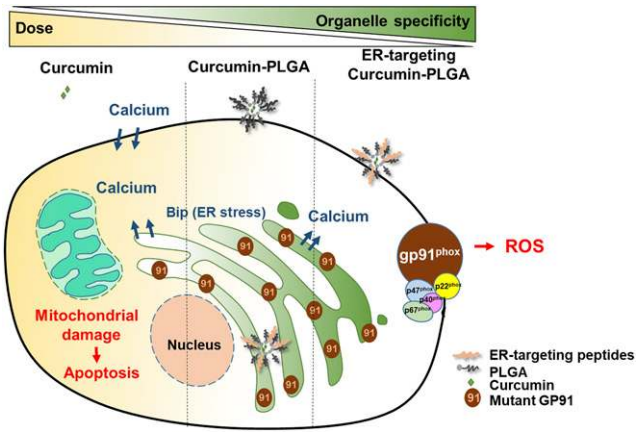

FIGURE 7. ER-targeting nanovehicle-encapsulated curcumin recovers the NOX2 function by rescuing the mutant gp91^{phox} protein and preventing treatment-induced apoptosis. Free curcumin at an effective concentration for SERCA inhibition may lead to ER stress and cell death induced by rapid calcium surge (left side of the figure). In contrast, ER-targeting NP-encapsulated curcumin at a lower concentration may induce equivalent ER calcium depletion and recover NOX2 function without excessive damage to the cell viability (right side of the figure).

Many inherited diseases, including nephrogenic diabetes insipidus and cystic fibrosis, are caused by the ER retention of misfolded mutant proteins (28). Misfolded proteins accumulate in the ER and lead to ER stress (29). To handle the accumulated proteins and ER stress, UPR is initiated in the cells expressing the mutant proteins. In UPR, chaperone proteins including Bip, calnexin, and calreticulin retain misfolded proteins that may then successfully undergo proteolysis. However, UPR may also aggravate cell dysfunction and even lead to cell death due to ER stress in many cases (30, 31). Based on the fact that the interaction of chaperones with misfolded proteins is Ca^{2+} dependent (32–34), SERCA inhibitors, including thapsigargin and curcumin, have been used to reduce ER calcium concentration, which leads to lower chaperone activity and allows the mutant proteins to escape from the ER (12). Previous studies showed that ΔF508 cystic fibrosis transmembrane conductance regulator (CFTR), similar to H338Y-gp91^{phox}, becomes functional if it can be released from ER after treatment with thapsigargin or curcumin (35, 36). However, the toxicity issue of thapsigargin made it challenging to use this drug as a clinical treatment (37). In this study, we aimed to find a new way of treatment with curcumin to modulate ER calcium homeostasis to regulate ER UPR response and facilitate the maturation of the mutant proteins. We used a novel CGD mouse model in which an ER-retained mutant H338Y-gp91phox protein is expressed in the leukocytes to show that in vivo ER-targeting curcumin-loaded PLGA NP treatment enhanced the leukocyte ROS production and bacterial clearance ability. Our results showed that delivery of curcumin with ER-targeting peptide decoration enhances the expression of the gp91^{phox} protein (Fig. 6). Moreover, we documented that ER-targeting curcumin-loaded PLGA NP effectively lowered ER stress when compared with nondecorated curcumin-loaded PLGA NP. These results suggest that selective delivery of curcumin to the ER region is a superior way to alter ER calcium homeostasis and restore leukocyte functions when compared with other ways of delivery.

Curcumin is a natural compound derived from *Curcuma longa* that has been known as a SERCA inhibitor and reported to be a promising drug candidate for many different diseases (38, 39). However, curcumin is poorly water-soluble and is degraded rapidly in the body (40). Several studies indicated that high doses of curcumin intake did not elevate blood curcumin levels in healthy volunteers (41). Thus, bioavailability is among the most crucial issues that need to be addressed before curcumin can be used effectively as a drug for systemic diseases. Researchers have been focusing on improving the bioavailability through different approaches, including identifying new curcumin analogs and developing novel drug delivery systems. The NP-based delivery system has been used to enhance the bioavailability of hydrophobic chemicals (42, 43). Curcumin delivery with NPs was previously shown to improve absorption with increased concentration in the blood circulation (41, 44). PLGA forms biodegradable polymers with minimal toxicity and has been approved by the U.S. Food and Drug Administration in various drug delivery systems in humans (45). Moreover, it was shown that most of the PLGA NPs in the bloodstream are engulfed by phagocytes, which are the primary cell type that produces the gp91^{phox} protein (46). PLGA nanovehicle delivery hence is a reasonable system to deliver curcumin to H338Y-gp91^{phox}–expressing neutrophils in CGD. By using PLGA NPs containing curcumin, we were able to enhance the efficacy of curcumin as a SERCA inhibitor to deplete ER calcium contents (Fig. 3). To further improve its pharmacological function as an inhibitor of SERCA, which is expressed on the ER membrane, we decorated the NPs with KDEL peptide for ER-targeted delivery of curcumin (Fig. 2). Although NP curcumin both with or without ER targeting increased the efficiency of calcium depletion from the ER (Fig. 3), we were able to show significant enhancement in H338Y-gp91^{phox} expression in *Cybb*^{C1024T} transgenic *Cybb*$^{-/-}$ mice treated with ER-targeting curcumin-loaded PLGA NP in the biochemical analysis (Fig. 6). Localizing the curcumin intracellular administration by NP encapsulation, therefore, appears to have the expected beneficial effects in rescuing the mutant protein while lowering the overall dosage of the treatment.

Cellular Ca^{2+} homeostasis is pivotal in maintaining cellular functions including proliferation, signal transduction, migration, and cell death (47–50). To support the homeostasis, ER serves as a Ca^{2+} reservoir that keeps cytoplasmic Ca^{2+} concentration at a low level. One of the essential Ca^{2+} channels that sustain ER Ca^{2+} content is SERCA, which retrieves Ca^{2+} from the cytoplasm to the ER lumen (48). Inhibition of SERCA function hence depletes ER Ca^{2+} content and consequently induces extracellular calcium entry and leads to elevation of cytoplasm Ca^{2+} level. The transient elevation flux of cytoplasmic calcium level then serves as a second messenger that facilitates cellular signal transduction (51). However, the prolonged high concentration of Ca^{2+} in the cytoplasm may lead to ER stress, ERK phosphorylation, mitochondrial damage, and cell death (48, 52). The intracellular calcium fluctuation-induced cytotoxicity may become a limiting factor when using SERCA inhibitors as drugs (48, 53). In our study, we found that NP encapsulation not only promotes curcumin-mediated ER calcium release but also delays the extracellular calcium entry (Fig. 4). Consequently, the overall calcium levels in curcumin-loaded PLGA NP-treated cells were lowered. It was previously reported that curcumin treatment may inhibit extracellular calcium entry (54, 55). Our results, however, showed that extracellular calcium entry was reduced in cells treated with curcumin-loaded PLGA NPs but not in cells treated with free curcumin. The findings in this study suggest that localizing curcumin to the intracellular regions close to ER may critically modulate the role of curcumin as a regulator of cellular calcium mobilization. Previous studies have shown that the interaction between plasma membrane calcium release-activated channel (CRAC) and ER calcium sensor stromal interaction molecule 1 (STIM1) is crucial for the extracellular calcium entry induced by

ER calcium depletion (49, 51, 56). Given that STIM1 is localized to the junction between the ER and plasma membrane, whether the organelle-targeting delivery of curcumin to the ER region reduces the STIM1/CRAC interaction and delays the extracellular calcium entry should be further investigated.

Based on our results showing that NP encapsulation lowers curcumin-induced mitochondrial damage and cellular apoptosis (Fig. 5), we reason that the delayed and reduced calcium influx induced by encapsulated curcumin may contribute to the improved cell survival of the treated cells. Therefore, modulation of intracellular curcumin distribution and hence the kinetics of calcium by NP encapsulation may have the beneficial effects in rescuing the functions of the mutant immune cells not only through rescuing the mutant protein from the ER but also through decreasing the unintended cell death caused by of the treatment. Our in vivo verification using a mouse model carrying an equivalent mutation on the CYBB gene which leads to a phenotype corresponding to human CGD patients may expedite the use of this novel treatment in human diseases.

In conclusion, our study showed that organelle-targeting NP encapsulation improves the bioavailability and efficacy of curcumin as a SERCA inhibitor to rescue the ER-retained H338Y- $gp91^{phox}$ protein compared with free-form curcumin. As ER not only plays essential roles in cellular biosynthesis but also participates in different cellular functions including protein quality control, calcium homeostasis, and cell viability, our formulation of ER-targeting NP vehicles for drug delivery promises to be a novel approach to treat certain PIDD including CGD.

Acknowledgments

We thank Dr. Wen-Tai Chiu (Department of Biomedical Engineering, NCKU, Tainan, Taiwan) for the helpful discussion. The authors gratefully acknowledge the JEM-2100F of the machine equipment belonging to the Instrument Development Center of the NCKU, and we are grateful to the Center for Clinical Medicine Research (Institute of Clinical Medicine, NCKU Medical College) and the National Synchrotron Radiation Research Center (Hsinchu, Taiwan) for the help of confocal images and FTIR measurements.

Disclosures

The authors have no financial conflicts of interest.

References

1. O'Neill, S., J. Brault, M. J. Stasia, and U. G. Knaus. 2015. Genetic disorders coupled to ROS deficiency. *Redox Biol.* 6: 135–156.
2. Roos, D. 2016. Chronic granulomatous disease. *Br. Med. Bull.* 118: 50–63.
3. Holland, S. M. 2013. Chronic granulomatous disease. *Hematol. Oncol. Clin. North Am.* 27: 89–99, viii.
4. Nguyen, G. T., E. R. Green, and J. Mecsas. 2017. Neutrophils to the ROScue: mechanisms of NADPH oxidase activation and bacterial resistance. *Front. Cell. Infect. Microbiol.* 7: 373.
5. Huang, Y. F., P. C. Lo, C. L. Yen, P. A. Nigrovic, W. C. Chao, W. Z. Wang, G. C. Hsu, Y. S. Tsai, and C. C. Shieh. 2015. Redox regulation of pro-IL-1β processing may contribute to the increased severity of serum-induced arthritis in NOX2-deficient mice. *Antioxid. Redox Signal.* 23: 973–984.
6. Huang, C., S. S. De Ravin, A. R. Paul, T. Heller, N. Ho, L. Wu Datta, C. S. Zerbe, B. E. Marciano, D. B. Kuhns, H. A. Kader, et al; NIDDK IBD Genetics Consortium. 2016. Genetic risk for inflammatory bowel disease is a determinant of crohn's disease development in chronic granulomatous disease. *Inflamm. Bowel Dis.* 22: 2794–2801.
7. Chiriaco, M., I. Salfa, G. Di Matteo, P. Rossi, and A. Finocchi. 2016. Chronic granulomatous disease: clinical, molecular, and therapeutic aspects. *Pediatr. Allergy Immunol.* 27: 242–253.
8. Ochs, H. D., and D. Petroni. 2018. From clinical observations and molecular dissection to novel therapeutic strategies for primary immunodeficiency disorders. *Am. J. Med. Genet. A.* 176: 784–803.
9. Marciano, B. E., and S. M. Holland. 2017. Primary immunodeficiency diseases: current and emerging therapeutics. *Front. Immunol.* 8: 937.
10. Arnold, D. E., and J. R. Heimall. 2017. A review of chronic granulomatous disease. *Adv. Ther.* 34: 2543–2557.
11. Lin, S. J., Y. F. Huang, J. Y. Chen, P. G. Heyworth, D. Noack, J. Y. Wang, C. Y. Lin, B. L. Chiang, C. M. Yang, C. C. Liu, and C. C. Shieh. 2002. Molecular quality control machinery contributes to the leukocyte NADPH oxidase deficiency in chronic granulomatous disease. *Biochim. Biophys. Acta* 1586: 275–286.
12. Egan, M. E., J. Glöckner-Pagel, C. Ambrose, P. A. Cahill, L. Pappoe, N. Balamuth, E. Cho, S. Canny, C. A. Wagner, J. Geibel, and M. J. Caplan. 2002. Calcium-pump inhibitors induce functional surface expression of Delta F508-CFTR protein in cystic fibrosis epithelial cells. *Nat. Med.* 8: 485–492.
13. Huang, Y. F., S. Y. Liu, C. L. Yen, P. W. Yang, and C. C. Shieh. 2009. Thapsigargin and flavin adenine dinucleotide ex vivo treatment rescues trafficking-defective gp91phox in chronic granulomatous disease leukocytes. *Free Radic. Biol. Med.* 47: 932–940.
14. Bilmen, J. G., S. Z. Khan, M. H. Javed, and F. Michelangeli. 2001. Inhibition of the SERCA Ca2+ pumps by curcumin. Curcumin putatively stabilizes the interaction between the nucleotide-binding and phosphorylation domains in the absence of ATP. *Eur. J. Biochem.* 268: 6318–6327.
15. Wang, L., L. Wang, R. Song, Y. Shen, Y. Sun, Y. Gu, Y. Shu, and Q. Xu. 2011. Targeting sarcoplasmic/endoplasmic reticulum Ca^2+-ATPase 2 by curcumin induces ER stress-associated apoptosis for treating human liposarcoma. *Mol. Cancer Ther.* 10: 461–471.
16. Seo, J. A., B. Kim, D. N. Dhanasekaran, B. K. Tsang, and Y. S. Song. 2016. Curcumin induces apoptosis by inhibiting sarco/endoplasmic reticulum Ca2+ ATPase activity in ovarian cancer cells. *Cancer Lett.* 371: 30–37.
17. Egan, M. E., M. Pearson, S. A. Weiner, V. Rajendran, D. Rubin, J. Glöckner-Pagel, S. Canny, K. Du, G. L. Lukacs, and M. J. Caplan. 2004. Curcumin, a major constituent of turmeric, corrects cystic fibrosis defects. *Science* 304: 600–602.
18. Gupta, S. C., B. Sung, J. H. Kim, S. Prasad, S. Li, and B. B. Aggarwal. 2013. Multitargeting by turmeric, the golden spice: from kitchen to clinic. *Mol. Nutr. Food Res.* 57: 1510–1528.
19. Reuter, S., S. Eifes, M. Dicato, B. B. Aggarwal, and M. Diederich. 2008. Modulation of anti-apoptotic and survival pathways by curcumin as a strategy to induce apoptosis in cancer cells. *Biochem. Pharmacol.* 76: 1340–1351.
20. Liu, H., J. Yang, L. Li, W. Shi, X. Yuan, and L. Wu. 2016. The natural occurring compounds targeting endoplasmic reticulum stress. *Evid. Based Complement. Alternat. Med.* 2016: 7831282.
21. Anand, P., A. B. Kunnumakkara, R. A. Newman, and B. B. Aggarwal. 2007. Bioavailability of curcumin: problems and promises. *Mol. Pharm.* 4: 807–818.
22. Naksuriya, O., S. Okonogi, R. M. Schiffelers, and W. E. Hennink. 2014. Curcumin nanoformulations: a review of pharmaceutical properties and preclinical studies and clinical data related to cancer treatment. *Biomaterials* 35: 3365–3383.
23. Cartiera, M. S., E. C. Ferreira, C. Caputo, M. E. Egan, M. J. Caplan, and W. M. Saltzman. 2010. Partial correction of cystic fibrosis defects with PLGA nanoparticles encapsulating curcumin. *Mol. Pharm.* 7: 86–93.
24. Zhong, Q., D. M. Chinta, S. Pamujula, H. Wang, X. Yao, T. K. Mandal, and R. B. Luftig. 2010. Optimization of DNA delivery by three classes of hybrid nanoparticle/DNA complexes. *J. Nanobiotechnology* 8: 6.
25. Gallagher, W. 2009. FTIR analysis of protein structure. In *Course manual Chem*, 455. Available at: https://www.chem.uwec.edu/Chem455_S05/Pages/Manuals/FTIR_of_proteins.pdf.
26. Bhattacharya, A., Q. Wei, J. N. Shin, E. Abdel Fattah, D. L. Bonilla, Q. Xiang, and N. T. Eissa. 2015. Autophagy is required for neutrophil-mediated inflammation. *Cell Rep.* 12: 1731–1739.
27. Chavakis, T., A. Bierhaus, N. Al-Fakhri, D. Schneider, S. Witte, T. Linn, M. Nagashima, J. Morser, B. Arnold, K. T. Preissner, and P. P. Nawroth. 2003. The pattern recognition receptor (RAGE) is a counterreceptor for leukocyte integrins: a novel pathway for inflammatory cell recruitment. *J. Exp. Med.* 198: 1507–1515.
28. Brooks, D. A. 1997. Protein processing: a role in the pathophysiology of genetic disease. *FEBS Lett.* 409: 115–120.
29. Hartl, F. U., A. Bracher, and M. Hayer-Hartl. 2011. Molecular chaperones in protein folding and proteostasis. *Nature* 475: 324–332.
30. Llewellyn, D. H., J. M. Kendall, F. N. Sheikh, and A. K. Campbell. 1996. Induction of calreticulin expression in HeLa cells by depletion of the endoplasmic reticulum Ca2+ store and inhibition of N-linked glycosylation. *Biochem. J.* 318: 555–560.
31. Winnay, J. N., J. Boucher, M. A. Mori, K. Ueki, and C. R. Kahn. 2010. A regulatory subunit of phosphoinositide 3-kinase increases the nuclear accumulation of X-box-binding protein-1 to modulate the unfolded protein response. *Nat. Med.* 16: 438–445.
32. Coe, H., and M. Michalak. 2009. Calcium binding chaperones of the endoplasmic reticulum. *Gen. Physiol. Biophys.* 28: F96–F103.
33. Nigam, S. K., A. L. Goldberg, S. Ho, M. F. Rohde, K. T. Bush, and Sherman MYu.1994. A set of endoplasmic reticulum proteins possessing properties of molecular chaperones includes Ca(2+)-binding proteins and members of the thioredoxin superfamily. *J. Biol. Chem.* 269: 1744–1749.
34. Charonis, A. S., M. Michalak, J. Groenendyk, and L. B. Agellon. 2017. Endoplasmic reticulum in health and disease: the 12th international calreticulin workshop, delphi, Greece. *J. Cell. Mol. Med.* 21: 3141–3149.
35. Egan, M. E., E. M. Schwiebert, and W. B. Guggino. 1995. Differential expression of ORCC and CFTR induced by low temperature in CF airway epithelial cells. *Am. J. Physiol.* 268: C243–C251.
36. Rubenstein, R. C., M. E. Egan, and P. L. Zeitlin. 1997. In vitro pharmacologic restoration of CFTR-mediated chloride transport with sodium 4-phenylbutyrate in cystic fibrosis epithelial cells containing delta F508-CFTR. *J. Clin. Invest.* 100: 2457–2465.

37. Wei, H., W. Wei, D. E. Bredesen, and D. C. Perry. 1998. Bcl-2 protects against apoptosis in neuronal cell line caused by thapsigargin-induced depletion of intracellular calcium stores. *J. Neurochem.* 70: 2305–2314.
38. Mekahli, D., G. Bultynck, J. B. Parys, H. De Smedt, and L. Missiaen. 2011. Endoplasmic-reticulum calcium depletion and disease. *Cold Spring Harb. Perspect. Biol.* 3: a004317.
39. Pulido-Moran, M., J. Moreno-Fernandez, C. Ramirez-Tortosa, and M. Ramirez-Tortosa. 2016. Curcumin and health. *Molecules* 21: 264.
40. Nelson, K. M., J. L. Dahlin, J. Bisson, J. Graham, G. F. Pauli, and M. A. Walters. 2017. The essential medicinal chemistry of curcumin. *J. Med. Chem.* 60: 1620–1637.
41. Hu, B., X. Liu, C. Zhang, and X. Zeng. 2017. Food macromolecule based nanodelivery systems for enhancing the bioavailability of polyphenols. *Yao Wu Shi Pin Fen Xi* 25: 3–15.
42. Salvia-Trujillo, L., O. Martín-Belloso, and D. J. McClements. 2016. Excipient nanoemulsions for improving oral bioavailability of bioactives. *Nanomaterials (Basel)* 6: E17.
43. Cheng, J., B. A. Teply, I. Sherifi, J. Sung, G. Luther, F. X. Gu, E. Levy-Nissenbaum, A. F. Radovic-Moreno, R. Langer, and O. C. Farokhzad. 2007. Formulation of functionalized PLGA-PEG nanoparticles for in vivo targeted drug delivery. *Biomaterials* 28: 869–876.
44. Shome, S., A. D. Talukdar, M. D. Choudhury, M. K. Bhattacharya, and H. Upadhyaya. 2016. Curcumin as potential therapeutic natural product: a nanobiotechnological perspective. *J. Pharm. Pharmacol.* 68: 1481–1500.
45. Danhier, F., E. Ansorena, J. M. Silva, R. Coco, A. Le Breton, and V. Préat. 2012. PLGA-based nanoparticles: an overview of biomedical applications. *J. Control. Release* 161: 505–522.
46. Gustafson, H. H., D. Holt-Casper, D. W. Grainger, and H. Ghandehari. 2015. Nanoparticle uptake: the phagocyte problem. *Nano Today* 10: 487–510.
47. Cui, C., R. Merritt, L. Fu, and Z. Pan. 2017. Targeting calcium signaling in cancer therapy. *Acta Pharm. Sin. B* 7: 3–17.
48. Chemaly, E. R., L. Troncone, and D. Lebeche. 2018. SERCA control of cell death and survival. *Cell Calcium* 69: 46–61.
49. Clemens, R. A., and C. A. Lowell. 2015. Store-operated calcium signaling in neutrophils. *J. Leukoc. Biol.* 98: 497–502.
50. Pinto, M. C., A. H. Kihara, V. A. Goulart, F. M. Tonelli, K. N. Gomes, H. Ulrich, and R. R. Resende. 2015. Calcium signaling and cell proliferation. *Cell. Signal.* 27: 2139–2149.
51. Prakriya, M., and R. S. Lewis. 2015. Store-Operated calcium channels. *Physiol. Rev.* 95: 1383–1436.
52. Li, D. W., J. P. Liu, Y. W. Mao, H. Xiang, J. Wang, W. Y. Ma, Z. Dong, H. M. Pike, R. E. Brown, and J. C. Reed. 2005. Calcium-activated RAF/MEK/ERK signaling pathway mediates p53-dependent apoptosis and is abrogated by alpha B-crystallin through inhibition of RAS activation. *Mol. Biol. Cell* 16: 4437–4453.
53. Sehgal, P., P. Szalai, C. Olesen, H. A. Praetorius, P. Nissen, S. B. Christensen, N. Engedal, and J. V. Møller. 2017. Inhibition of the sarco/endoplasmic reticulum (ER) Ca^{2+}-ATPase by thapsigargin analogs induces cell death via ER Ca^{2+} depletion and the unfolded protein response. *J. Biol. Chem.* 292: 19656–19673.
54. Shin, D. H., E. Y. Seo, B. Pang, J. H. Nam, H. S. Kim, W. K. Kim, and S. J. Kim. 2011. Inhibition of Ca2+-release-activated Ca2+ channel (CRAC) and K+ channels by curcumin in Jurkat-T cells. *J. Pharmacol. Sci.* 115: 144–154.
55. Kliem, C., A. Merling, M. Giaisi, R. Köhler, P. H. Krammer, and M. Li-Weber. 2012. Curcumin suppresses T cell activation by blocking Ca2+ mobilization and nuclear factor of activated T cells (NFAT) activation. *J. Biol. Chem.* 287: 10200–10209.
56. Chang, C.-L., Y.-J. Chen, C. G. Quintanilla, T.-S. Hsieh, and J. Liou. 2018. EB1 binding restricts STIM1 translocation to ER-PM junctions and regulates store-operated Ca^{2+} entry. *J. Cell Biol.* 217: 2047–2058.